

# Elsevier instructions for the preparation of a 1-column format camera-ready paper in L<sup>A</sup>T<sub>E</sub>X

P. de Groot<sup>a\*</sup>, R. de Maas<sup>a†</sup>, X.-Y. Wang<sup>b</sup> and A. Sheffield<sup>a‡</sup>

<sup>a</sup>Mathematics and Computer Science Section, Elsevier Science B.V.,  
P.O. Box 103, 1000 AC Amsterdam, The Netherlands

<sup>b</sup>Economics Department, University of Winchester,  
2 Finch Road, Winchester, Hampshire P3L T19, United Kingdom

These pages provide you with an example of the layout and style which we wish you to adopt during the preparation of your paper. Your text will be photographically reduced by 20–25%. This is the output from the L<sup>A</sup>T<sub>E</sub>X document class you requested.

## 1. FORMAT

Text should be produced within the dimensions shown on these pages: total width of 16 cm and a maximum length of 21 cm on first pages and 23 cm on second and following pages. The L<sup>A</sup>T<sub>E</sub>X document class uses the maximum stipulated length apart from the following two exceptions (i) L<sup>A</sup>T<sub>E</sub>X does not begin a new section directly at the bottom of a page, but transfers the heading to the top of the next page; (ii) L<sup>A</sup>T<sub>E</sub>X never (well, hardly ever) exceeds the length of the text area in order to complete a section of text or a paragraph. Here are some references: [ 1, 2].

### 1.1. Spacing

We normally recommend the use of 1.0 (single) line spacing. However, when typing complicated mathematical text L<sup>A</sup>T<sub>E</sub>X automatically increases the space between text lines in order to prevent sub- and superscript fonts overlapping one another and making your printed matter illegible.

### 1.2. Fonts

These instructions have been produced using a 12 point Computer Modern Roman. Other recommended fonts are 12 point Times Roman, New Century Schoolbook, Bookman Light and Palatino.

---

\*Footnotes should appear on the first page only to indicate your present address (if different from your normal address), research grant, sponsoring agency, etc. These are obtained with the \thanks command.

†For following authors with the same address use the \addressmark command.

‡To reuse an addressmark later on, label the address with an optional argument to the \address command, e.g. \address[MCSD], and repeat the label as the optional argument to the \addressmark command, e.g. \addressmark[MCSD].

## 2. PRINTOUT

The most suitable printer is a laser or an inkjet printer. A dot matrix printer should only be used if it possesses an 18 or 24 pin printhead (“letter-quality”).

The printout submitted should be an original; a photocopy is not acceptable. Please make use of good quality plain white A4 (or US Letter) paper size. *The dimensions shown here should be strictly adhered to: do not make changes to these dimensions, which are determined by the document class.* The document class leaves at least 3 cm at the top of the page before the head, which contains the page number.

Printers sometimes produce text which contains light and dark streaks, or has considerable lighting variation either between left-hand and right-hand margins or between text heads and bottoms. To achieve optimal reproduction quality, the contrast of text lettering must be uniform, sharp and dark over the whole page and throughout the article.

If corrections are made to the text, print completely new replacement pages. The contrast on these pages should be consistent with the rest of the paper as should text dimensions and font sizes.

## 3. TABLES AND ILLUSTRATIONS

Tables should be made with  $\text{\LaTeX}$ ; illustrations should be originals or sharp prints. They should be arranged throughout the text and preferably be included *on the same page as they are first discussed*. They should have a self-contained caption and be positioned in flush-left alignment with the text margin. Two small illustrations may be placed alongside one another as shown with Figures 1 and 2. All illustrations will undergo the same reduction as the text.

### 3.1. Tables

Tables should be presented in the form shown in Table 1. Their layout should be consistent throughout.

Table 1

The next-to-leading order (NLO) results *without* the pion field.

$\Lambda$ (MeV)	140	150	175	200
$r_d$ (fm)	1.973	1.972	1.974	1.978
$Q_d$ (fm <sup>2</sup> )	0.259	0.268	0.287	0.302
$P_D$ (%)	2.32	2.83	4.34	6.14
$\mu_d$	0.867	0.864	0.855	0.845
$\mathcal{M}_{M1}$ (fm)	3.995	3.989	3.973	3.955
$\mathcal{M}_{GT}$ (fm)	4.887	4.881	4.864	4.846
$\delta_{1B}^{VP}$ (%)	-0.45	-0.45	-0.45	-0.45
$\delta_{1B}^{C2:C}$ (%)	0.03	0.03	0.03	0.03
$\delta_{1B}^{C2:N}$ (%)	-0.19	-0.19	-0.18	-0.15

The experimental values are given in ref. [ 4].

Horizontal lines should be placed above and below table headings, above the subheadings and at the end of the table above any notes. Vertical lines should be avoided.

If a table is too long to fit onto one page, the table number and headings should be repeated above the continuation of the table. For this you have to reset the table counter with `\addtocounter{table}{-1}`. Alternatively, the table can be turned by 90° ('landscape mode') and spread over two consecutive pages (first an even-numbered, then an odd-numbered one) created by means of `\begin{table}[h]` without a caption. To do this, you prepare the table as a separate L<sup>A</sup>T<sub>E</sub>X document and attach the tables to the empty pages with a few spots of suitable glue.

### 3.2. Useful table packages

Modern L<sup>A</sup>T<sub>E</sub>X comes with several packages for tables that provide additional functionality. Below we mention a few. See the documentation of the individual packages for more details. The packages can be found in L<sup>A</sup>T<sub>E</sub>X's `tools` directory.

**array** Various extensions to L<sup>A</sup>T<sub>E</sub>X's `array` and `tabular` environments.

**longtable** Automatically break tables over several pages. Put the table in the `longtable` environment instead of the `table` environment.

**dcolumn** Define your own type of column. Among others, this is one way to obtain alignment on the decimal point.

**tabularx** Smart column width calculation within a specified table width.

**rotating** Print a page with a wide table or figure in landscape orientation using the `sidewaystable` or `sidewaysfigure` environments, and many other rotating tricks. Use the package with the `figuresright` option to make all tables and figures rotate in clockwise. Use the starred form of the `sideways` environments to obtain full-width tables or figures in a two-column article.

### 3.3. Line drawings

Line drawings may consist of laser-printed graphics or professionally drawn figures attached to the manuscript page, correctly aligned. They should be placed either at the bottom or at the top of the page. In the latter case the top of the figure should be at the same level as the first text line.

All notations and lettering should be no less than 2.5 mm high. The use of heavy black, bold lettering should be avoided as this will look unpleasantly dark when printed. Do not use too light or too dark *shading* in your figures. The pages will be reduced to 75–80% of their present size; too dark a shading may become too dense while a very light shading made of tiny points may fade away during reproduction.

### 3.4. PostScript figures

Instead of providing separate drawings or prints of the figures you may also use PostScript files which are included into your L<sup>A</sup>T<sub>E</sub>X file and printed together with the text. Use one of the packages from L<sup>A</sup>T<sub>E</sub>X's `graphics` directory: `graphics`, `graphicx` or `epsfig`, with the `\usepackage` command, and then use the appropriate commands (`\includegraphics` or `\epsfig`) to include your PostScript file.

Table 2: The next-to-leading order (NLO) results *without* the pion field.

$\Lambda$ (MeV)	140	150	175	200	225	250	Exp.	$v_{18}$ [?]
$r_d$ (fm)	1.973	1.972	1.974	1.978	1.983	1.987	1.966(7)	1.967
$Q_d$ (fm <sup>2</sup> )	0.259	0.268	0.287	0.302	0.312	0.319	0.286	0.270
$P_D$ (%)	2.32	2.83	4.34	6.14	8.09	9.90	—	5.76
$\mu_d$	0.867	0.864	0.855	0.845	0.834	0.823	0.8574	0.847
$\mathcal{M}_{M1}$ (fm)	3.995	3.989	3.973	3.955	3.936	3.918	—	3.979
$\mathcal{M}_{GT}$ (fm)	4.887	4.881	4.864	4.846	4.827	4.810	—	4.859
$\delta_{1B}^{VP}$ (%)	-0.45	-0.45	-0.45	-0.45	-0.45	-0.44	—	-0.45
$\delta_{1B}^{C2:C}$ (%)	0.03	0.03	0.03	0.03	0.03	0.03	—	0.03
$\delta_{1B}^{C2:N}$ (%)	-0.19	-0.19	-0.18	-0.15	-0.12	-0.10	—	-0.21

The experimental values are given in ref. [ 4].

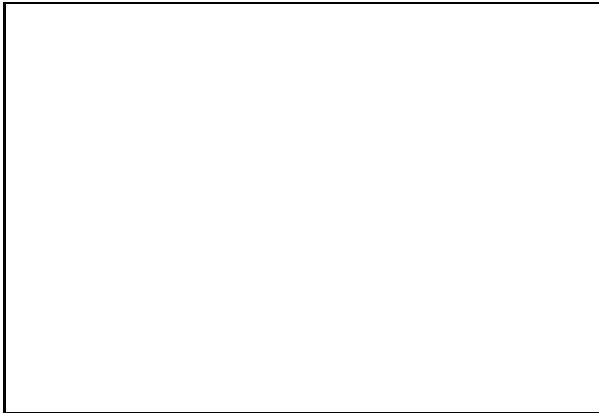


Figure 1. Good sharp prints should be used and not (distorted) photocopies.

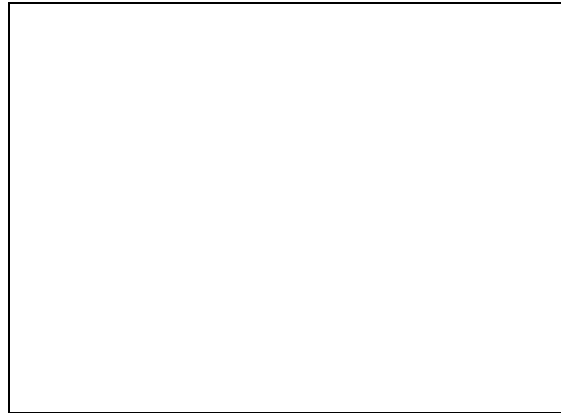


Figure 2. Remember to keep details clear and large enough to withstand a 20–25% reduction.

The simplest command is: `\includegraphics{file}`, which inserts the PostScript file `file` at its own size. The starred version of this command: `\includegraphics*{file}`, does the same, but clips the figure to its bounding box.

With the `graphicx` package one may specify a series of options as a key–value list, e.g.:

```
\includegraphics[width=15pc]{file}
\includegraphics[height=5pc]{file}
\includegraphics[scale=0.6]{file}
\includegraphics[angle=90,width=20pc]{file}
```

See the file `grfguide`, section “Including Graphics Files” of the `graphics` distribution for all options and a detailed description.

The `epsfig` package mimicks the commands familiar from the package with the same name in L<sup>A</sup>T<sub>E</sub>X2.09. A PostScript file `file` is included with the command  
`\psfig{file=file}`.

Grey-scale and colour photographs cannot be included in this way, since reproduction from the printed CRC article would give insufficient typographical quality. See the following subsections.

### 3.5. Black and white photographs

Photographs must always be sharp originals (*not screened versions*) and rich in contrast. They will undergo the same reduction as the text and should be pasted on your page in the same way as line drawings.

### 3.6. Colour photographs

Sharp originals (*not transparencies or slides*) should be submitted close to the size expected in publication. Charges for the processing and printing of colour will be passed on to the author(s) of the paper. As costs involved are per page, care should be taken in the selection of size and shape so that two or more illustrations may be fitted together on one page. Please contact the Author Support Department at Elsevier (E-mail:

[authorsupport@elsevier.nl](mailto:authorsupport@elsevier.nl)) for a price quotation and layout instructions before producing your paper in its final form.

#### 4. EQUATIONS

Equations should be flush-left with the text margin; L<sup>A</sup>T<sub>E</sub>X ensures that the equation is preceded and followed by one line of white space. L<sup>A</sup>T<sub>E</sub>X provides the document class option `fleqn` to get the flush-left effect.

$$H_{\alpha\beta}(\omega) = E_{\alpha}^{(0)}(\omega)\delta_{\alpha\beta} + \langle\alpha|W_{\pi}|\beta\rangle \quad (1)$$

You need not put in equation numbers, since this is taken care of automatically. The equation numbers are always consecutive and are printed in parentheses flush with the right-hand margin of the text and level with the last line of the equation. For multi-line equations, use the `eqnarray` environment.

For complex mathematics, use the *AMSmath* package. This package sets the math indentation to a positive value. To keep the equations flush left, either load the `espcrc` package *after* the *AMSmath* package or set the command `\mathindent=0pt` in the preamble of your article.

#### REFERENCES

1. S. Scholes, Discuss. Faraday Soc. No. 50 (1970) 222.
2. O.V. Mazurin and E.A. Porai-Koshits (eds.), Phase Separation in Glass, North-Holland, Amsterdam, 1984.
3. Y. Dimitriev and E. Kashchieva, J. Mater. Sci. 10 (1975) 1419.
4. D.L. Eaton, Porous Glass Support Material, US Patent No. 3 904 422 (1975).

References should be collected at the end of your paper. Do not begin them on a new page unless this is absolutely necessary. They should be prepared according to the sequential numeric system making sure that all material mentioned is generally available to the reader. Use `\cite` to refer to the entries in the bibliography so that your accumulated list corresponds to the citations made in the text body.

Above we have listed some references according to the sequential numeric system [1, 2, 3, 4].

# High $p_T$ Measurements from PHENIX

S. Mioduszewski<sup>a</sup> for the PHENIX Collaboration\*

<sup>a</sup>Physics Department, Brookhaven National Laboratory, Upton, NY 11973, USA

We present recent high transverse momentum measurements by the PHENIX experiment for Au+Au and p+p collisions at  $\sqrt{s_{NN}} = 200$  GeV at the Relativistic Heavy Ion Collider (RHIC). We show particle spectra for neutral pions and charged hadrons, define and show the nuclear modification factor, and discuss particle composition. By means of the nuclear modification factor, we observe a suppression factor of 5-6 for neutral pions and 3-4 for charged hadrons in central collisions at high  $p_T$ . We find that the ratio of  $\pi^0$  to  $(h^+ + h^-)/2$  remains nearly constant at  $\sim 0.5$  for  $p_T = 2 - 9$  GeV/c. Finally we present strong evidence for the observation of jets in Au+Au collisions.

## 1. Introduction

In Run II at RHIC ( $\sqrt{s_{NN}} = 200$  GeV), PHENIX has been able to measure particle yields up to large transverse momenta,  $p_T \sim 10$  GeV/c, where the cross section is expected to be dominated by hard processes. This high statistics data set allows us to study the systematics of high  $p_T$  phenomena in detail and at much higher  $p_T$  than possible in Run I ( $\sqrt{s_{NN}} = 130$  GeV) data.

In p+p collisions, it is known that hard scattering and the fragmentation of the scattered partons dominates the production of hadrons above  $p_T \sim 2$  GeV/c [ 1]. In Au+Au collisions, these hard scatterings are of particular interest because they occur early in the collision, leaving the hard-scattered partons sensitive to the properties of the collision medium. Further interactions of these partons in the dense medium might cause the high transverse momentum tail of the hadron spectrum, where the hadrons are likely to be the leading particles of jets, to be suppressed [ 2]. Due to the high multiplicity environment, jets cannot be directly observed in a heavy ion collision. We can however determine the contribution of jet fragmentation to hadron yields at high  $p_T$  via correlation measurements and use this knowledge to interpret the measured hadron  $p_T$  spectra.

First, we give a brief overview of the PHENIX detector. In the following sections, we proceed assuming that the hadrons at high  $p_T$  emanate from jets, with the objective of measuring the effect of the dense medium on the hard-scattered partons through modification of the particle spectra at high  $p_T$ . We define the nuclear modification factor and show such a quantity for both neutral pions and charged hadrons. With the measurement of spectra for both charged hadrons and neutral pions, we also investigate the particle

---

\*for the full PHENIX Collaboration author list and acknowledgements, see Appendix “Collaborations” of this volume.

composition at high  $p_T$ . Finally, we use two-particle correlations to test the assumption that the high  $p_T$  hadrons are due to the fragmentation of hard-scattered partons.

## 2. Overview of the PHENIX Detector

PHENIX is a versatile detector, with tracking chambers, ring-imaging Cerenkov (RICH) detectors, a time-of-flight (TOF) wall, and electromagnetic calorimeters in the central arms, which cover  $\Delta\eta = \pm 0.35$  and  $180^\circ$  in azimuth. Along the beamline there are beam-beam counters and zero-degree calorimeters, which are used for event triggering and centrality classification. Neutral pions are measured via their  $\gamma\gamma$ -decay using the electromagnetic calorimeters (EMCal). There are 6 sectors of Lead-Scintillator (PbSc) and 2 sectors of Lead-Glass (PbGl) calorimeter, providing two independent measurements of the  $\pi^0$   $p_T$  spectrum. The charged hadron spectrum is measured using the tracking detectors: drift chambers and pad chambers. At  $p_T$  above  $\sim 5$  GeV/c the RICH detector, together with an energy cut in the PbSc, is used to identify charged pions. With various detection methods, PHENIX can make multiple overlapping measurements at high  $p_T$ , providing valuable consistency checks. Details of the detector are described elsewhere [3].

## 3. High $p_T$ Particle Spectra

In Run II, PHENIX recorded more than 30 million minimum bias Au+Au events. This event sample enables us to reach 10 GeV/c in the transverse momentum spectra of both identified neutral pions and charged hadrons. In addition, we recorded 140 million p+p events in which we measure neutral pions up to 13 GeV/c. Shown in Fig. 1 is the neutral pion production cross section as a function of  $p_T$ , measured with the PbSc, for p+p collisions [4]. The measured p+p spectrum is compared to a fit to UA1 data [5] over the range  $p_T < 6$  GeV/c, extrapolated to higher  $p_T$ . Although our measurement agrees with the UA1 data, it disagrees with this extrapolation at very high  $p_T$ . This new measurement provides an important reference spectrum for comparison with the Au+Au data.

For Au+Au collisions, the events are binned into centrality selections, and the spectra are shown for the most central bin and a peripheral bin in Figs. 2 and 3. Centrality is expressed as a percentage of the total inelastic cross section. In the Run II data, the charged hadron yields are measured up to  $p_T = 10$  GeV/c for central events and  $p_T = 5$  GeV/c for peripheral events, while the neutral pion yields are measured up to 8 and 6.5 GeV/c for central and peripheral events respectively.

## 4. $R_{AA}$ for Neutral Pions

The nuclear modification factor quantifies the effect of A+A compared to p+p collisions on particle yields for point-like processes. It is defined as the ratio of the particle yield in a A+A collision to the yield in a p+p collision scaled by the mean number of binary (nucleon+nucleon) collisions  $N_{coll}$  in the A+A event sample. Because hard processes are generally believed to scale with  $N_{coll}$  (“binary-scaling”), this ratio is expected to be one

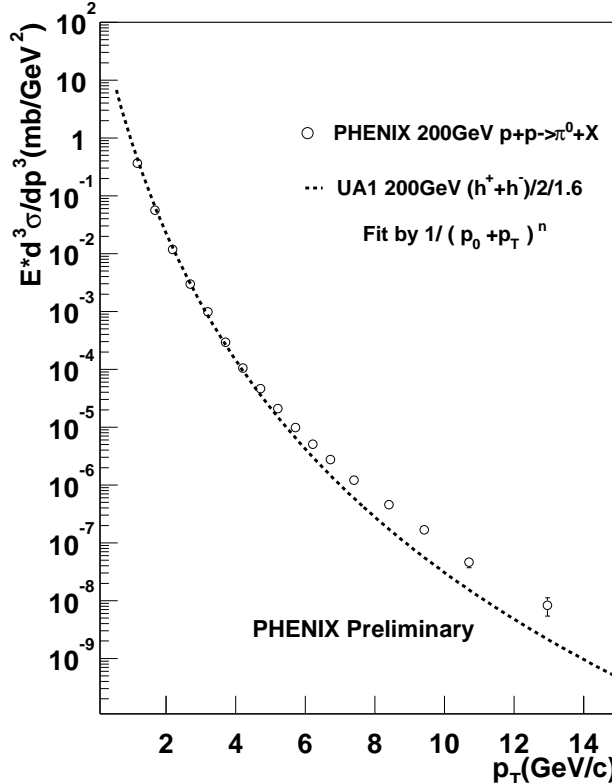


Figure 1. Neutral pion production cross section vs.  $p_T$  in  $p+p$  collisions at  $\sqrt{s_{NN}} = 200$  GeV.

at high  $p_T$  in the absence of any nuclear effects.

$$R_{AA}(p_T) = \frac{(\text{Yield per A + A collision})}{\langle N_{coll} \rangle (\text{Yield per p + p collision})} = \frac{d^2 N^{A+A} / dp_T d\eta}{\langle N_{coll} \rangle (d^2 \sigma^{p+p} / dp_T d\eta) / \sigma_{inelastic}^{p+p}}. \quad (1)$$

Shown in Fig. 4 is  $R_{AA}$  as a function of  $p_T$  for central  $\text{Pb}+\text{Pb}$  collisions at  $\sqrt{s_{NN}} = 17$  GeV from WA98 [8] and central  $\text{Au}+\text{Au}$  collisions at  $\sqrt{s_{NN}} = 130$  GeV from PHENIX Run I [9]. Already in this comparison, the suppression relative to binary-scaling at 130 GeV is striking. It is quite different from the enhancement observed at 17 GeV. This enhancement is known as the “Cronin effect” [10] and has been attributed to  $p_T$  broadening due to initial state scatterings [11, 12]. Figure 5 shows  $R_{AA}$  for central and peripheral  $\text{Au}+\text{Au}$  collisions at  $\sqrt{s_{NN}} = 200$  GeV. The central data again show a suppression as seen at 130 GeV. With a measurement that extends to much larger  $p_T$ , the suppression is shown to persist up to  $p_T \sim 8$  GeV/c and is as much as a factor of 5-6 at the largest  $p_T$ . The measurement of the  $p+p$  reference spectrum with the same detector greatly reduces the systematic error in  $R_{AA}$  for central events. The  $R_{AA}$  for peripheral events is consistent with binary-scaling ( $p+p$  yields scaled by the number of binary collisions in the peripheral event sample). The error in this ratio is dominated by the uncertainty in  $\langle N_{coll} \rangle$  for peripheral collisions. Within the rather large errors, the spectrum for peripheral collisions does not show effects of the nuclear medium. If there is a Cronin effect at RHIC, it is not strongly evident in peripheral collisions.

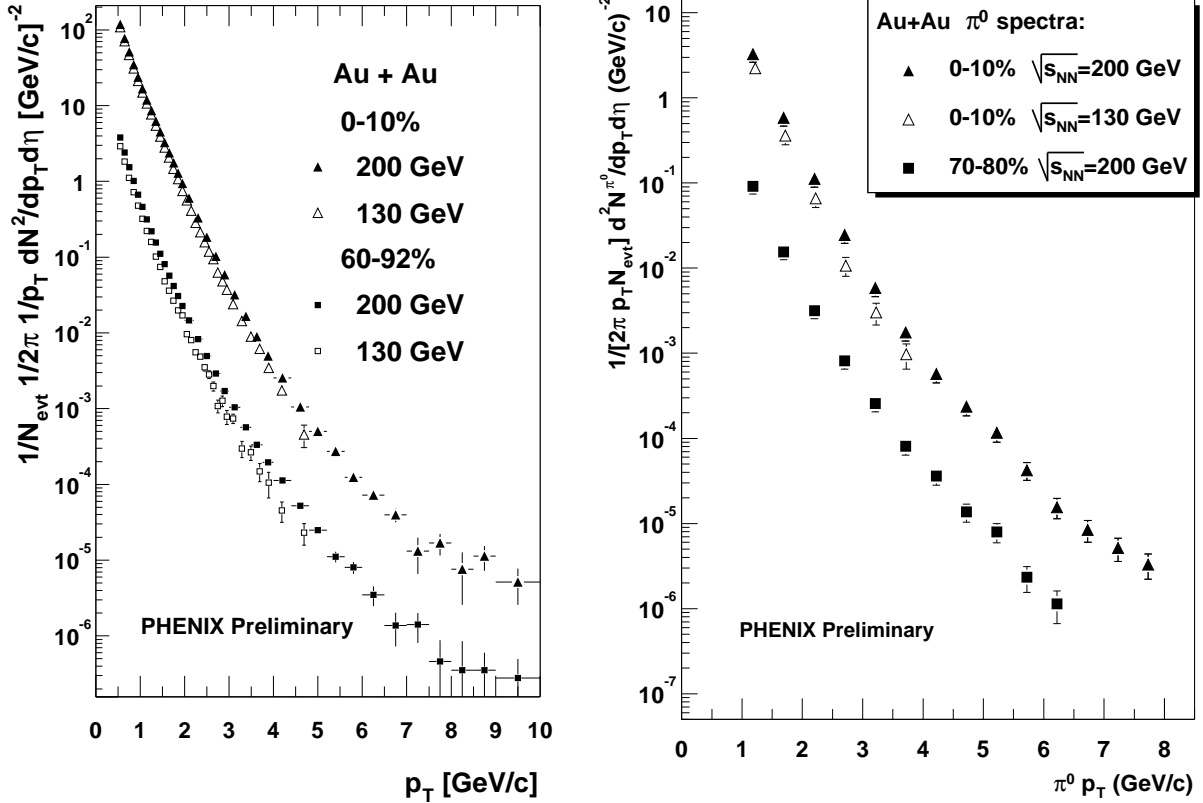


Figure 2. Invariant yields of  $(h^+ + h^-)/2$  as a function of  $p_T$  in Au+Au collisions at  $\sqrt{s_{NN}} = 200$  GeV [ 6] and 130 GeV for centrality selections of 0-10% and 60-92%.

Figure 3. Invariant yields of  $\pi^0$  as a function of  $p_T$  in Au+Au collisions at  $\sqrt{s_{NN}} = 200$  GeV and 130 GeV for centrality 0-10% and  $\sqrt{s_{NN}} = 200$  GeV for centrality 70-80%.

There are a number of model predictions, shown in Fig. 6, that were made prior to the release of the Run II data. In the case of one model which assumes energy loss that is constant with respect to the parton's energy [ 12],  $R_{AA}$  increases by a factor of  $\sim 2$  from  $p_T \sim 3.5$  to  $p_T \sim 8$  GeV/c. Although the magnitude of the suppression qualitatively describes the data at  $p_T \sim 4$  GeV/c, the increasing  $R_{AA}$  with  $p_T$  is contrary to what is observed in central Au+Au collisions. Two other models which use a common formalism for including energy-dependent energy loss differ in the point where the calculation is begun (thus resulting in somewhat different predictions). One such model predicts an  $R_{AA}$  that increases only slightly with increasing  $p_T$  [ 13], while another model predicts a nearly constant  $R_{AA}$  from  $p_T \sim 4$  to at least  $p_T \sim 10$  GeV/c [ 14]. The energy-dependent energy loss models give reasonable agreement with the data. This is also seen in another calculation made subsequent to the release of the Run II data [ 15].

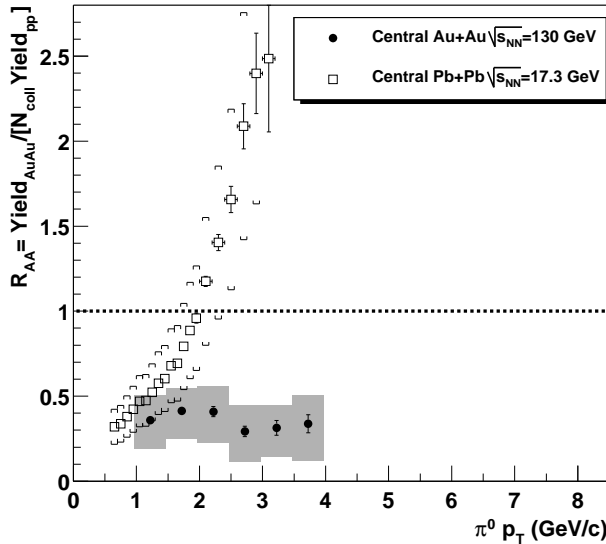


Figure 4.  $R_{AA}(\pi^0)$  for central Pb+Pb collisions at  $\sqrt{s_{NN}} = 17$  GeV and central Au+Au collisions at  $\sqrt{s_{NN}} = 130$  GeV. The error bars are the statistical  $\oplus p_T$ -dependent systematic errors. The brackets/boxes are the errors on the normalization of this ratio.

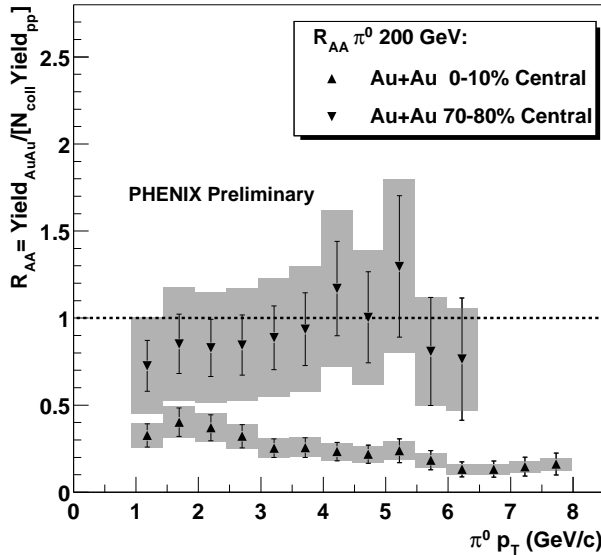


Figure 5.  $R_{AA}(\pi^0)$  for central and peripheral Au+Au collisions at  $\sqrt{s_{NN}} = 200$  GeV. The error bars are the statistical  $\oplus p_T$ -dependent systematic errors. The shaded boxes are the errors on the normalization of the ratio.

## 5. Comparison of Central Collisions with Respect to Peripheral Collisions

An alternate measure of the nuclear modification is the central-to-peripheral ratio scaled by the number of binary collisions,

$$\text{Binary-Scaled Central/Peripheral} = \frac{(\text{Yield per central collision})/\langle N_{\text{coll}}^{\text{central}} \rangle}{(\text{Yield per peripheral collision})/\langle N_{\text{coll}}^{\text{peripheral}} \rangle}. \quad (2)$$

Since the  $\pi^0$  spectrum in peripheral Au+Au collisions is consistent with the binary-scaled p+p  $\pi^0$  spectrum (Fig. 5), this ratio is similar to  $R_{AA}$ . An advantage of this ratio is that many of the systematic uncertainties in the measurement cancel, particularly for charged hadrons. A disadvantage is that it is sensitive to the centrality dependence of the Cronin effect, which is not known. Figure 7 shows this ratio as a function of  $p_T$  for neutral pions, charged hadrons, and charged pions. The suppression is observed in all three measurements. In the charged hadrons, the suppression factor reaches 3-4 at high  $p_T$ . The difference in this ratio between the identified pions and charged hadrons seems to be due to the particle composition. In particular, we find that  $p/\pi^0 \sim 1$  in central collisions for  $p_T = 2 - 4$  GeV/c while  $p/\pi^0 \sim 0.4$  in peripheral collisions [16]. The error in the normalization, denoted by a shaded area for the charged hadrons and outlines for the neutral pions, is dominated by the uncertainty in  $\langle N_{\text{coll}} \rangle$  for peripheral collisions.

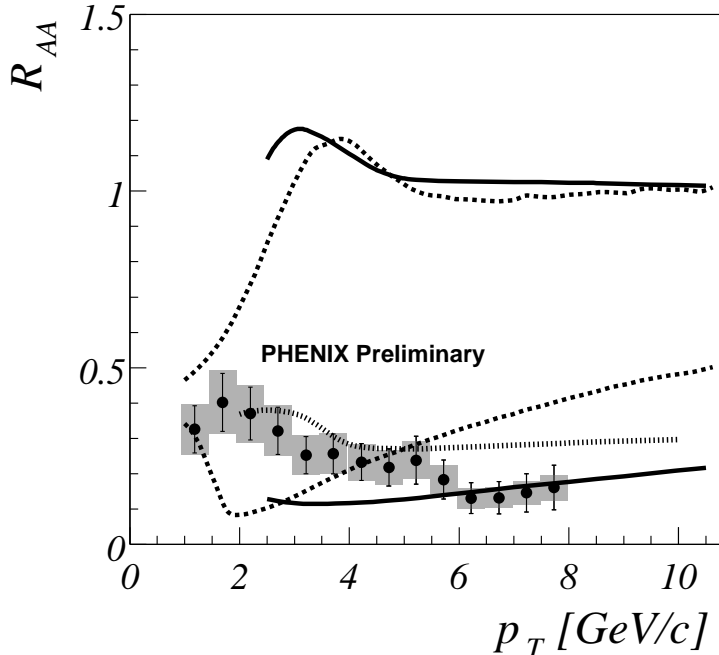


Figure 6.  $R_{AA}$  as a function of  $p_T$  compared to theoretical predictions for central Au+Au collisions at  $\sqrt{s_{NN}} = 200$  GeV. The dotted lines are predictions with and without energy loss (constant) [ 12]. The solid lines are again predictions with and without energy loss (energy-dependent) [ 13], and the hashed line is also a prediction with energy-dependent energy loss [ 14].

## 6. Centrality Dependence of $R_{AA}$

As shown in Fig. 5, the 10% most central events have a suppression factor reaching 5-6, while the 70-80% centrality selection is consistent with binary-scaled p+p collisions. We now address the evolution of the nuclear modification factor from the most peripheral to the most central collisions, in terms of the mean number of participating nucleons  $N_{part}$  in a centrality selection. For the 10% most central collisions,  $\langle N_{part} \rangle = 327$ , and for the 70-80% central collisions,  $\langle N_{part} \rangle = 14$ . Figure 8 shows  $R_{AA}$  vs.  $N_{part}$  for neutral pions with  $4 < p_T < 6$  GeV/c. The suppression gradually increases from peripheral to central events. The same trend is seen in the charged hadron yields. Figure 9 shows the integrated yield scaled by  $N_{coll}$  vs.  $N_{part}$  for charged hadrons. This quantity is similar to  $R_{AA}$ , differing only in normalization by the p+p reference yields. Again the binary-scaled yield decreases, or the suppression increases, gradually with increasing  $N_{part}$ .

## 7. Particle Composition at High $p_T$

PHENIX can measure the  $p/\pi$  ratio up to almost 4 GeV/c in  $p_T$  [ 16], at which point protons can no longer be distinguished from other particles via their time of flight. Since neutral pions are identified to much higher  $p_T$ , we can look at the ratio of  $\pi^0$  to nonidentified charged hadrons ( $h^+ + h^-$ )/2 for  $p_T > 4$  GeV/c. This ratio is shown in Fig. 10 for minimum bias events. The surprising feature that this ratio does not increase for trans-

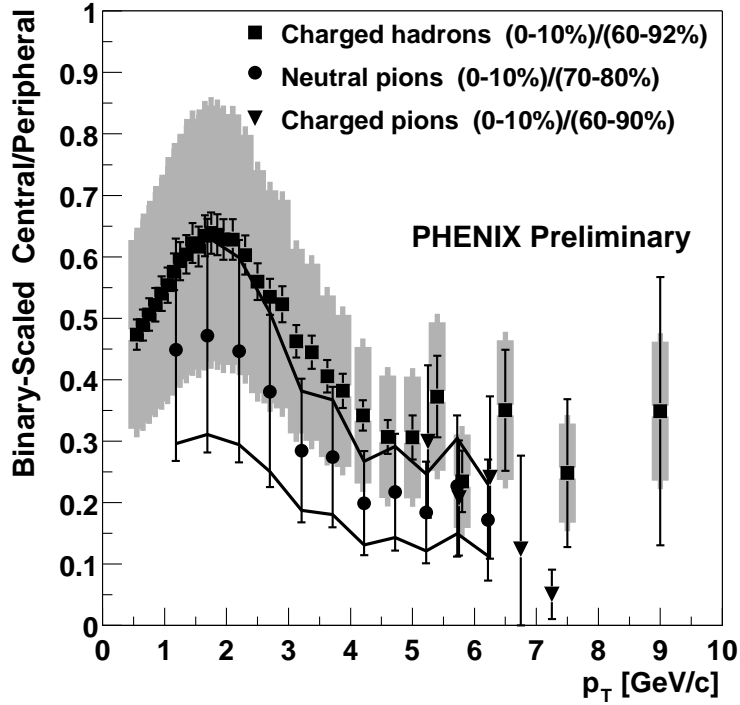


Figure 7. Binary-scaled central-to-peripheral ratio vs.  $p_T$  for charged hadrons, neutral pions, and charged pions measured in Au+Au collisions. The error bars are statistical  $\oplus p_T$ -dependent systematic errors. The error in the overall normalization is shown as outlines for neutral pions and a shaded area for charged hadrons. For charged pions, the error is dominated by statistics.

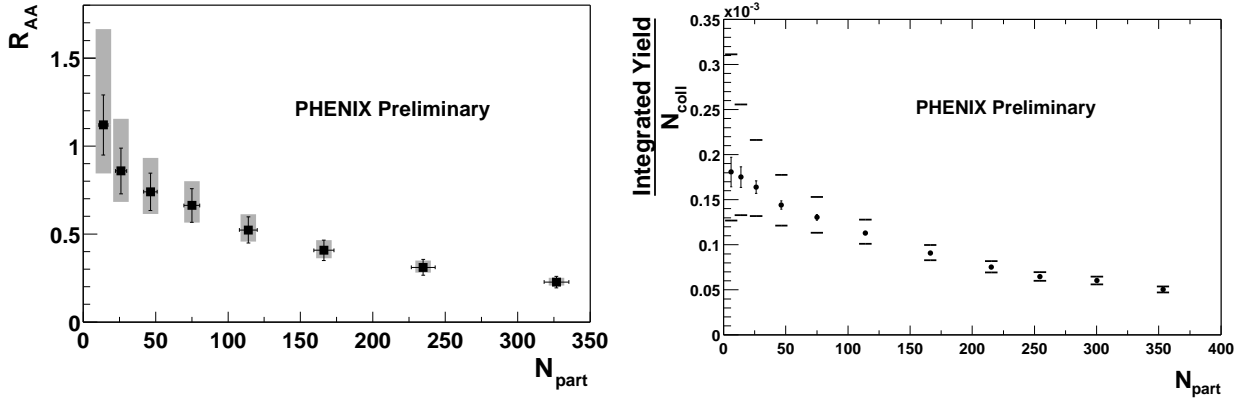


Figure 8.  $R_{AA}$  vs.  $N_{part}$  (or centrality of the collision) for neutral pions with  $4 < p_T < 6$  GeV/c. The shaded boxes denote the error on  $\langle N_{coll} \rangle$ . There is an additional error of 20% in the overall normalization that is not shown.

Figure 9. Integrated yield scaled by  $N_{coll}$  vs.  $N_{part}$  for charged hadrons with  $p_T > 4$  GeV/c. The brackets denote the error on  $\langle N_{coll} \rangle$ .

verse momenta greater than 4 GeV/c, but remains nearly constant at a value around 0.5, indicates that approximately half of the charged hadrons at high  $p_T$  are protons and/or kaons, assuming  $\pi^0 = (\pi^+ + \pi^-)/2$ . This result is rather different from hard processes as measured in  $e^+e^-$  collisions [ 17]. The interpretation for this new result is not yet clear. There may be some other production mechanism for protons and/or kaons in Au+Au collisions at these large transverse momenta. Alternatively, the large proton and/or kaon content at high  $p_T$  could be due to a difference in the suppression of pions relative to protons/kaons.

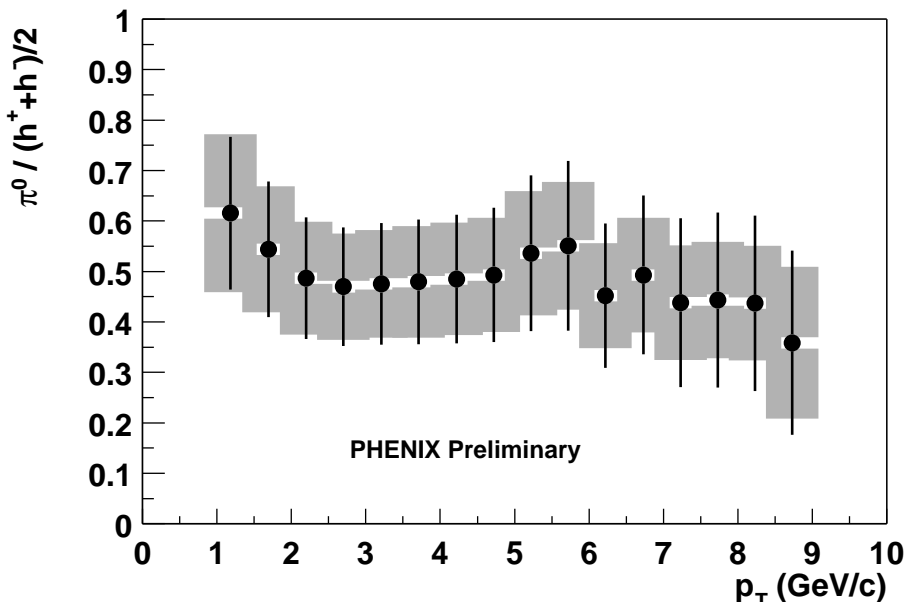


Figure 10. Ratio of  $\pi^0$  to  $(h^+ + h^-)/2$  as a function of  $p_T$  for minimum bias Au+Au collisions.

## 8. Evidence for Jets

Since jets cannot be directly observed in a Au+Au collisions, a correlation analysis is required to detect their presence. We take a high  $p_T$  neutral particle, a cluster in the EMCAL with energy greater than 2.5 GeV, as the trigger and correlate it with all charged particles in the event within a given range in  $p_T$ . Comparing the correlations that we measure in p+p collisions at  $\sqrt{s_{NN}} = 200$  GeV to those from the PYTHIA event generator [ 18], we establish that PYTHIA reproduces the behavior of jets known to be present in p+p collisions. PYTHIA is then compared to Au+Au collisions at  $\sqrt{s_{NN}} = 200$  GeV, which demonstrates that the correlations we observe in Au+Au collisions behave as expected for jets, both in the azimuthal and polar angles. Figure 11 shows the background-subtracted correlation in the azimuthal angle  $\Delta\phi$  of the trigger particle with charged particles having  $p_T$  between 2 and 4 GeV/c. Also shown is a fit to the data of the correlation produced by PYTHIA with an added  $\cos(2\phi)$  term. The  $\cos(2\phi)$  term accounts for the contribution of flow to the correlation, while the coefficient of the PYTHIA term represents the

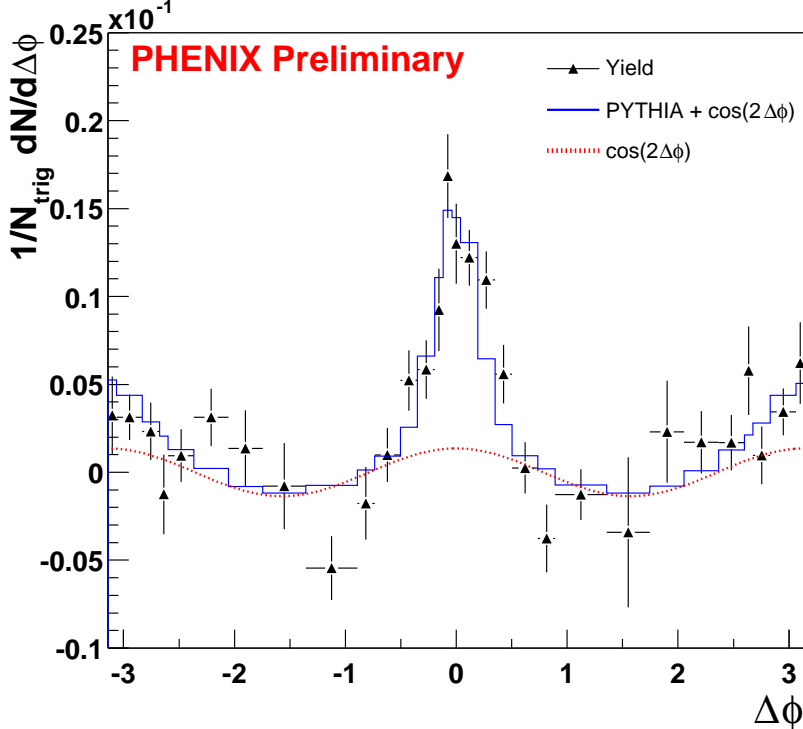


Figure 11. Acceptance-corrected yield (in 20-40% centrality selection) fit to PYTHIA plus an elliptic flow term.

contribution due to jets. Further details of this analysis are given elsewhere [ 19]. From the figure, one can see that much of the correlation can be attributed to jets (PYTHIA), particularly the near-side correlation around  $\Delta\phi = 0$ . The trigger particle is typically a photon from a  $\pi^0$  decay. This is strong evidence that when we trigger on a high  $p_T \pi^0$ , we are indeed looking at a leading particle from a jet.

## 9. Conclusions

We have presented  $p_T$  spectra for charged hadrons in Au+Au collisions and neutral pions in Au+Au and p+p collisions and have shown that the high  $p_T$  suppression observed in Run I RHIC data at  $\sqrt{s_{NN}} = 130$  GeV [ 9, 20] persists up to  $p_T \sim 8$  GeV/c at  $\sqrt{s_{NN}} = 200$  GeV. The neutral pions are suppressed by a factor of 5-6 and the charged hadrons by 3-4 for  $p_T > 4$  GeV/c in the most central collisions. The suppression increases gradually with increasing centrality, or  $N_{part}$ . We have also shown that when triggering on a high  $p_T$  neutral particle, which is predominantly a photon from a  $\pi^0$  decay, the correlation between the neutral and charged particles in the event is jet-like. This is strong evidence that the neutral pions that we measure at high  $p_T$  indeed have significant contributions from jet fragmentation. Finally, we have shown that approximately half of the charged hadrons at high  $p_T$  are not pions, but protons and/or kaons, up to  $p_T \sim 9$  GeV/c.

## REFERENCES

1. J.F. Owens *et al.*, Phys. Rev. **D18**, 1501 (1978).

2. M. Gyulassy and M. Plümer, Phys. Lett. **B243**, 432 (1990); R. Baier *et al.*, Phys. Lett. **B345**, 277 (1995); X.N. Wang and M. Gyulassy, Phys. Rev. Lett. **68**, 1480 (1992); X.N. Wang, Phys. Rev. **C58**, 2321 (1998).
3. PHENIX Collaboration, D. Morrison, *et al.*, Nucl. Phys. **A638**, 565c (1998); PHENIX Collaboration, W. Zajc, *et al.*, Quark Matter 2001.
4. H. Torii for the PHENIX Collaboration, these proceedings.
5. C. Albajar *et al.*, Nucl. Phys. **B335**, 261 (1990).
6. J. Jia for the PHENIX Collaboration, these proceedings.
7. D. D'Enterria for the PHENIX Collaboration, these proceedings.
8. M.M. Aggarwal *et al.* [WA98 Collaboration], Eur. Phys. J. **C23** (2002) 225-236.
9. K. Adcox *et al.* [PHENIX Collaboration], Phys. Rev. Lett. **88**, 022301 (2002).
10. D. Antreasyan *et al.*, Phys. Rev. **D19**, 764 (1979).
11. M. Lev and B. Petersson, Z. Phys. **C21**, 155 (1983); T. Ochiai *et al.*, Prog. Theor. Phys. **75**, **288** (1986).
12. X.N. Wang, Phys. Rev. **C61**, 064910 (2000).
13. P. Levai *et al.*, Nuclear Physics **A698** (2002) 631.
14. I. Vitev and M. Gyulassy, these proceedings, hep-ph/0208108; M. Gyulassy, P. Levai and I. Vitev, Nucl. Phys. **B** 594, p. 371 (2001).
15. S. Jeon, J. Jalilian-Marian and I. Sarcevic, nucl-th/0208012.
16. T. Sakaguchi for the PHENIX Collaboration, these proceedings.
17. P. Abreu *et al.* [DELPHI Collaboration], Eur. Phys. J. **C17**, 207 (2000), DOI 10.1007/s100520000449.
18. T. Sjostrand, Comput. Phys. Commun. **82**, 74 (1994).
19. M. Chiu for the PHENIX Collaboration, these proceedings.
20. C. Adler *et al.* [STAR Collboration], nucl-ex/0206011.